Fusion of PET and MR Brain Images Based on IHS and Log-Gabor Transforms

Cheng-I Chen

***Abstract*— In medical imaging, positron emission tomography (PET) shows metabolic changes of an organism in pseudo color and magnetic resonance (MR) imaging presents anatomical structures in gray level. The PET and MR brain medical image fusion produces one composite image rendering the anatomical structures with metabolic changes to help doctors effectively diagnose a possible disease. For this purpose, a new fusion method based on Intensity-Hue-Saturation model and log-Gabor wavelet transform is proposed. First, MR image and the intensity component of PET image are decomposed by log-Gabor wavelet transform with suitable decomposition scale. Then, maximum selection' fusion rule for the high-frequency sub-band and two-stage fusion rule based on weighted-averaging scheme and visibility measure for the low-frequency sub-band are employed. Finally, a new intensity component, obtained by applying reverse log-Gabor wavelet transform to the fused high- and low-frequency sub-bands, along with original hue and saturation components of PET image are converted to obtain our fused color image. In our fused images, both anatomical structures and color changes are rendered with effectively-reduced color distortion. Experimental results on twelve sets, including normal axial, normal coronal, and Alzheimer's disease brain images, demonstrate that our fusion method outpaces framelet-transform-based method both visually and quantitatively.**

***Index Terms*— IHS model, log-Gabor wavelet transform, MR image, PET image, visibility measure.**

I. Introduction

INFORMATION and content in images of the same scene acquired from different sensor devices are often distinct and complementary for one another. By image fusion technique, the information from a series of images can be effectively integrated into one single informative image. This composite image has a better description of the scene than any single source image, and consequently more suitable for specific tasks, such as image processing, feature extraction, and target detection [1]–[4]. In addition, image fusion also provides a good solution to the reduction of data storage, and improves the image content reliability. Therefore, image fusion techniques have been widely developed and have become a potential researching field [5]–[12].

Over the past few decades, various image fusion techniques have been developed and applied to different application fields. In remote sensing field, high-spatial-resolution panchromatic image and low-spatial-resolution multispectral images are combined to acquire high-spatial-resolution images carrying spectral information. In defense or surveillance applications, visible images and thermal/infrared images are integrated to obtain a composite image. This composite image is a good medium for recognition tasks in a challenging environment of illumination variations [5], [6]. Another example is medical images fusion of different modalities carrying distinct and important information of an organism [7], [11], [12]. For instance, in traditional imaging, Magnetic Resonance (MR) imaging that displays high-spatial-resolution anatomical structures in gray level and Positron Emission Tomography (PET) that displays metabolic changes in pseudo color are demonstrated in two separated images. In diagnosis, doctors encounter difficulties in inspecting those two different images separately, as the MR image is essential to verify the location of a possible disease, and PET image is needed to observe the metabolic changes. Therefore, integrating the PET and MR medical images into one individual image can help doctors accurately diagnose a possible disease with less effort. Nevertheless, image registration is also a key factor that influences on the performance of the medical images fusion of different modalities. Therefore, before the fusion process begins, medical images of different modalities are required to be transformed by registration algorithm so that anatomical structures of the MR image would be well-aligned with the corresponding functional regions of the PET image. Methods of image registration have been reviewed and widely applied to different applications [13]–[16], and we are aware that image registration is undeniably the main challenge before fusion process. The research below assumes that original images are the same size and well-registered before fusion process.

Different effective image fusion methods have been presented in literatures. Methods based on statistical or numerical approaches, such as Principal Component Analysis (PCA), Intensity-Hue-Saturation model (IHS), Brovey Transform (BT) are firstly developed [11], [17]–[19]. PCA fusion method maximizes the variance in the fused image by finding the optimal weight for each source image [9], but it is a global method and cannot well handle local vibration of intensity changes in PET (color change) and MR images (anatomical structure).. The IHS-substitution method based on IHS model is first applied to remote sensing field to combine high-spatial-resolution panchromatic image and low-spatial-resolution multispectral image. In this method, low-spatial-resolution multispectral image is first transformed from Red (R), Green (G), and

Manuscript received July 21, 2017; accepted August 14, 2017. Date of publication August 30, 2017; date of current version October 11, 2017. The associate editor coordinating the review of this paper and approving it for publication was Prof. Danilo Demarchi.

The author is with the Computer Science and Engineering Department, National Chung Hsing University, Taichung City 402, Taiwan (e-mail: chenchengi2009@gmail.com).

Digital Object Identifier 10.1109/JSEN.2017.2747220

Blue (B) channels to Intensity (I), Hue (H), and Saturation (S) components by IHS model. Then, the I-component of multispectral image is replaced by the panchromatic image. Finally, the substitutive panchromatic image, along with unchanged H- and S-component of multispectral image, is transformed back to R, G, and B channels and then a high-spatial-resolution colorful image is obtained. IHS-substitution method is also applied to the fusion of PET and MR brain medical images and it can provide fused images with rich structural information, however, colors of fused images are distorted because the substitutive MR image is rather different from the replaced I-component of the PET image. Brovey-transform method multiplies each R, G, and B value of low-spatial-resolution colorful image with the intensity ratio of the high-spatial-resolution image and the low-spatial-resolution one, so that high-spatial-resolution information is introduced into the fused image. Although statistical and numerical approaches can produce fused images carrying rich spatial-resolution or anatomical information, but colors of fused images are distorted with different degree [19]. To reduce color distortion in fused images, multi-scale wavelet-transform-based methods are then proposed [17], [20]–[23]. First, source images are decomposed by multi-scale wavelet transform into high- and low-frequency sub-bands of different scales for advance fusion process. Then, each corresponding high-frequency (and low-frequency) sub-band from different images is combined by some fusion rule. Finally, the new set of high- and low-frequency sub-bands for the fused image is reversely wavelet transformed to obtain one composite image. There are two key factors that influence the fusion performance of wavelet-transform-based methods. One is how complete the high-frequency information is extracted from source images, and the other is the design of fusion rules for high- and low-frequency sub-bands. The visibility of color changes and anatomical structures in the fused images is highly related to the amount of the high-frequency information extracted from PET and MR images. The more complete the high-frequency information is extracted, the better the color changes and anatomical structures are rendered in the fused images. However, the high-frequency information of anatomical structures and color changes, which are not oriented in horizontal, vertical, and diagonal directions, is not well-extracted by traditional wavelet transform, so that the completeness of high-frequency information is unsatisfactory. To efficiently detect the high-frequency information from images, Contourlet Transform (CT) which increases the flexibility in directional decomposition is thereby developed [24]. The CT is a multi-directional and multi-scale transform constructed by Laplacian pyramid and Directional Filter Bank (DFB), but is not shift-invariant due to downsampling and upsampling steps in both the Laplacian pyramid and DFB. To eliminate deficiencies in the CT, Non-Subsampled Contourlet Transform (NSCT) which gets rid of the sampling steps during decomposition and reconstruction stages is further developed [24], [25]. The NSCT is a shift-invariance, multi-resolution and multi-dimensionality transform and has been widely applied to image denoising, image enhancement, as well as image fusion [25], [26]. In addition to CT and NSCT transform, Framelet Transform (FT) possessing two wavelet functions, whereas traditional wavelet transform has only one wavelet function, is also developed [27], [28]. Due to several desirable properties, such as near shift invariance, minimal or no error of reconstructed signals, more directionally selective for image processing, FT has been introduced into the framework of multi-modal medical image fusion and has shown outstanding fusion performance, especially in CT/MR images fusion [29]. However, decomposing images into high- and low-frequency sub-bands by using FT takes more time comparing to traditional wavelet transform, and resultant images obtained by FT-based methods exhibit serious color degradation.

Recently, to deal with the problems of traditional wavelet transform, the log-Gabor wavelet transform consisting of a logarithmic transformation of the Gabor filters has been proposed and widely investigated [30]–[33]. A Gabor filter is obtained by modulating a sinusoid with a Gaussian so that it responds to some frequency only in a localized part of the signal [30]. Gabor filters can simultaneously analyze space and frequency information and have been adopted as ideal functions for signal analysis and image processing where exact reconstruction is not required, such as edge extraction, texture analysis, object recognition and so on. Nevertheless, Gabor filters have some deficiencies that limit their performance in many application fields. Therefore, log-Gabor filters are then proposed to get rid of the problems annoying in Gabor filters [30], [32]. The log-Gabor filters have capability of making the bands more disjoined and minimizing DC component annoying in Gabor filters. Moreover, exact reconstruction, which is not possible in Gabor filters due to the usage of non-orthogonal bases, can be easily achieved by using complex conjugate of original log-Gabor filters. Due to these desirable properties, the wavelet transform based on log-Gabor filters provides a good tool for analyzing high- and low-frequency information of images and it have been applied to the fusion of multi-focus images [33]. In our study, we found that the log-Gabor wavelet transform is very suitable for the fusion of PET and MR brain images for two reasons. First, high-frequency information from anatomical structures of the MR image is extracted more completely by log-Gabor wavelet transform comparing to the traditional wavelet transform. As a result, preserving such high-frequency information in the fused image promotes the visibility of anatomical structures. Second, DC component in high-frequency information of MR image is obviously different from I-component of PET image, and adding high-frequency information carrying DC component of MR image into I-component of PET image to generate the substitutive I-component results in serious color distortion. However, the high-frequency information of MR image extracted by log-Gabor wavelet transform carries less DC component and adding such high-frequency information makes color changes of PET image present in fused images with less distortion. For these two reasons, we utilize log-Gabor wavelet transform in our proposed method to help construct fused images with less color distortion and rich anatomical structures.

In addition to the option of wavelet transform, the design of fusion rule for high- and low-frequency sub-bands is also a key factor that affects the final fusion performance.

Fusion rule aims to inject high-frequency information, such as edge, texture, and color changes, from source images into the composite image while reducing information distortion as better as possible. Therefore, the design of fusion rule is a key factor that influences the quality of resultant images.

In general, the IHS-substitution method based on IHS model can be fast implemented to integrate both color and spatial-resolution information from source images, but colors are seriously distorted in the fused images. On the contrary, traditional wavelet-transform-based methods generate fused images with less color distortion, but spatial-resolution or anatomical structural information in the fused images is unsatisfactory. To avoid weak points of traditional IHS-substitution methods and wavelet-transform-based methods, we put forward a new method for the fusion of PET and MR brain images based on IHS model and log-Gabor wavelet transform with suitable decomposition scale and fusion rules. Remaining sections present our proposed method, experimental results and performance comparisons, as well as our analysis and conclusion. In Section 2, IHS model and log-Gabor wavelet transform utilized in our proposed method is discussed in detail, and our proposed method based on IHS model and log-Gabor wavelet transform with suitable decomposition scales and fusion rules is also addressed. Experiments that demonstrate the outstanding performance of our method in visual comparison and quantitative metrics are presented in Section 3. Finally, conclusions are given in Section 4.

II. Materials and Methods

In this section, we briefly describe IHS-substitution method and log-Gabor wavelet transform which are utilized in our proposed method.

A. IHS-Substitution Method

The IHS-substitution method utilizes the principle of IHS model to generate composite images carrying distinct and complementary information from source images. First, the low-spatial-resolution colorful image is transformed from R, G, and B channels to I, H, and S components by IHS transform. I-component of low-spatial-resolution colorful image is then substituted by high-spatial-resolution gray-level image. The substitutive gray-level image, along with unchanged H- and S-component of low-spatial-resolution image, is transformed back to R, G, and B color channels and then a fused image is obtained. According to IHS model, the more the high-spatial-resolution gray-level image differs from the replaced I-component of low-spatial-resolution image, the more the colors in fused images are distorted. For the fusion of PET and MR brain images, IHS-substitution method also suffers from serious color distortion because the substitutive MR image is rather different from the replaced I-component of PET image. There is another intricate problem in IHS-substitution method, where the anatomical structures are unclear and may even disappear in fused images if the gray level of the pixels in the MR image is almost the same as that of the corresponding pixels in the I-component of the PET image. To overcome the problems of IHS-substitution method, the substitutive I-component should differ moderately from the original I-component of the PET image. For this purpose, our method generates the substitutive I-component with the help of log-Gabor wavelet transform which is described in detail as follow.

B. Log-Gabor Wavelet Transform

The log-Gabor wavelet transform consists of a logarithmic transformation of Gabor filters. A Gabor filter is obtained by modulating a sinusoid with a Gaussian, and thereby it responds to some frequency only in a localized part of the signal [30]. Gabor filters can simultaneously analyze space and frequency information and have been adopted as ideal functions for signal analysis and image processing. Gabor filters have been used as a tool for image processing and analysis where exact reconstruction is not required, such as edge extraction, texture analysis, object recognition and so on [30]. Nevertheless, Gabor filters have several drawbacks. Firstly, they overlap in the low frequencies more importantly than in the higher ones and thus lead to a non-uniform coverage of the Fourier domain. Secondly, they are affected by DC components as they have not zero mean. Thirdly, exact reconstruction is impossible due to the usage of non-orthogonal bases. To overcome these problems, log-Gabor filters are then proposed [31], [32]. The expression of log-Gabor filters in the log-polar coordinates of the Fourier domain is shown as follows:

$$G_{p,k}(\rho,\theta) = \exp\left(-\frac{1}{2}\left(\frac{\rho-\rho_k}{\sigma_\rho}\right)^2\right) \times \exp\left(-\frac{1}{2}\left(\left(\frac{\theta-\theta_{p,k}}{\sigma_\theta}\right)^2\right)\right) \quad (1)$$

in which (ρ,θ) are the log-polar coordinates (in log2 scale), p is the directional angle and k indexes the scale, the pair $(\rho_k,\theta_{p,k})$ corresponds to the coordinates of center of the filter, $(\sigma_\rho,\sigma_\theta)$ are bandwidths in (ρ,θ) and defined as $(\sigma_\rho,\sigma_\theta) = 0.996(\sqrt{\frac{2}{3}}, \frac{1}{\sqrt{2}}\frac{\pi}{n_t})$, where n_t is the number of orientations [31]. Once the number of orientations (directional angles) is selected, the bandwidths $(\sigma_\rho,\sigma_\theta)$ are thereby defined.

Suppose that the whole set of filters constructed by (1) are indexed by $\Omega = \{1,2,\ldots,n_p n_k+1\}$ with n_p and n_k being the number of orientation p and scale k, respectively, the filter set defined in the Fourier domain is then refereed as $\{G_s | s \in \Omega\}$. Let $h_s(I)$ be the convolution of the image I by any filter G_s, then $h_s(I)$ can be computed as $h_s(I) = F^{-1}(G_r \cdot F(I))$ with F and F^{-1} being the direct and inverse discrete Fourier transform, respectively. Thus, log-Gabor wavelet transform of an image I is defined as:

$$W(I) = (h_s(I))_{s\in\Omega} \quad (2)$$

and the inverse log-Gabor transform is defined as:

$$W^{-1}(h_s(I))_{s\in\Omega} = F^{-1}\left(\sum_{s\in\Omega}\overline{G_s}\cdot F(h_s(I))\right), \quad (3)$$

where $\overline{G_s}$ is the complex conjugate of G_s.

If we refer $h_s(I)$ as a decomposed channel by log-Gabor wavelet transformation of image I, then $\{h_s(I)|s \in \Omega\}$ is the whole set of decomposed channels that image I being filtered by each individual filter G_s in Ω and is the log-Gabor wavelet transformation of I. The image I, which can be obtained by the inverse transform of the filtered image, thus can be reconstructed from the combination of each inverse transformed decomposed channel $h_s(I)$, i.e., $z_s(I) = F^{-1}(\overline{G_s} \cdot F(h_s(I)))$. Hence, $Z_s(I)$ is referred as the reconstructed channel of $h_s(I)$, and the summation of all reconstructed channels is the reconstructed image $\overline{I}$:

$$\overline{I} = \sum_{s \in \Omega} z_s(I) \tag{4}$$

The multi-scale scheme is completed with a low-pass filter (approximation) for recovering the luminance information and filtering parameters are constrained by the design recommended in [31] for an exact reconstruction.

The log-Gabor wavelet transform is very suitable for the fusion of PET and MR brain images for two reasons. First, high-frequency information is more complete when being extracted by wavelet transform based on log-Gabor filters than Gabor filters [31], [32]. As a result, more complete high-frequency information from anatomical structures of the MR image is extracted and preserved in the fused image so that the visibility of anatomical structures is increased. Second, high-frequency information extracted by log-Gabor wavelet transform carries less DC component [31], [32]. Thus, color distortion from PET images will be reduced and visibility of anatomical structures will be increased in fused images.

For these two reasons, we utilize log-Gabor wavelet transform in our proposed method. The detail of our proposed method is described in the following subsection.

C. Our Proposed Method

Our goal is to devise a fusion method for a pair of gray scale MR image and a RGB pseudo color PET image so that the fused image can simultaneously preserve both spatial (anatomical structures in MR image) and spectral fidelity (colors in PET image), respectively, as much as possible.

As described in the above section, applying IHS substitution method to MR and PET images will produce a fused image with high spatial but poor spectral fidelity, while applying traditional wavelet-transform-based methods will generate fused images with better spectral fidelity but trading off spatial fidelity. Meanwhile, log-Gabor wavelet transform has been demonstrated with capabilities of extracting more complete high frequency information from the source image and exact reconstruction. Thus, we propose a fusion method that takes advantages of both IHS-substitution and log-Gabor wavelet transform methods for MR and PET images and denote it IHS+LG.

Our method firstly applies IHS transformation to the RGB PET image to intensity (I), hue (H), and saturation(S) components by IHS transform. Both the MR image and I-component of PET image are decomposed into high- and low-frequency sub-bands by log-Gabor wavelet transform with suitable decomposition scale. The corresponding high-frequency (and low-frequency) sub-band coefficients from MR image and I-component of PET image are integrated by our proposed fusion rules. Once all coefficients are processed, a new set of high-frequency (and low-frequency) sub-band coefficients for the fused image is then obtained. The complete set of new high- and low-frequency sub-band coefficients for the fused image is then inversely log-Gabor wavelet transformed to a new I-component. Finally, the new I-component, along with unchanged H- and S-component of PET image, is transformed back to R, G, and B channels and then a fused image is obtained. By our proposed fusion method, anatomical structures and color changes are appropriately rendered in fused images with less distortion. In our proposed fusion method, there are two key factors that deeply influence the performance of our proposed fusion method. One is the determination of decomposition scale and orientation for log-Gabor wavelet transform, the other is the design of fusion rules for high- and low-frequency sub-bands. We discuss these two key factors in detail in the following subsections.

1) Determination of Decomposition Scale and Orientation for Log-Gabor Wavelet Transform: The selection is based on an analysis on a 2-stage trial result. In stage-1 trial, we first selected decomposition scale 5 for both MR and PET images to be fused, knowing that too small scale cannot extract enough anatomical structure information from MR image to be processed. In order to accurately observe how much high-frequency information of MR image, which affects the visibility of anatomical structures in the fused image, is extracted by log-Gabor wavelet transform with different decomposition scales, the fusion rules for the low-frequency and high-frequency sub-bands is specially designed. For high-frequency sub-bands fusion, we directly select high-frequency sub-bands of MR image as those of the fused image. For low-frequency sub-band fusion, low-frequency sub-band of I-component of PET image is selected as that of the fused image to help us accurately observe fusion effect.

From the fused result, we found out that the anatomical structures in MR image are indeed rendered well; however, colors are noticeably lighter than the original PET. So we tried a smaller decomposition scale (=3) for the same pair of images, and found out that colors of the fused image were much closer to those in the original PET, but the anatomical structures in the highlighted (high frequency) region are not as clear as those in the original MRI. Fig.1 demonstrates the result of this trial, where Fig. 1 (a) and (b) are the MR and PET images to be fused, and Figs. 1 (c) and 1(d) show the fusion results of using a decomposition scale of 5 and 3, respectively. Thus, we conjecture that scale 4 might be a good choice for achieving acceptable result for both spatial and spectral fidelity.

We confirm this conjecture by proceeding to stage-2 trial. We tested 12 datasets of MR and PET images of different content, including normal axial, normal coronal and Alzheimer's disease brain images, using decomposition scale 3, 4, and 5, respectively. The fused images revealed consistent results as those from stage-1 test, i.e., both spatial and spectral fidelity were best achieved in fused images based on scale 4. Fig. 2 shows the results of three image data sets belonging

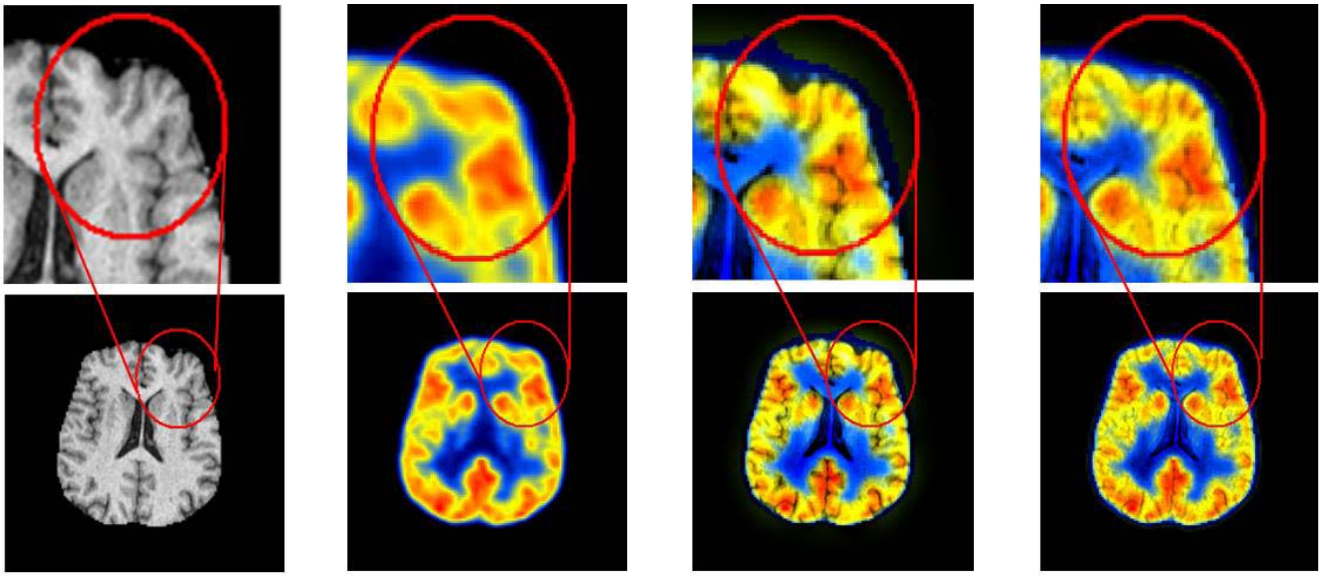

(a) (b) (c) (d)

Fig. 1. Fused results based on log-Gabor wavelet transform with different decomposition scales. (a) MR image. (b) PET image. (c) Fused result by using log-Gabor wavelet transform with decomposition scale 5. (d) Fused result by using log-Gabor wavelet transform with decomposition scale 3.

TABLE I

SPATIAL-QUALITY PERFORMANCE COMPARISON OF OUR FUSED IMAGES WITH DIFFERENT DIRECTIONAL ANGLES FOR LOG-GABOR WAVELET TRANSFORM IN TERMS OF AG AND ASD METRICS

Metric	Dir.	data set 01	data set 02	data set 03	data set 04	data set 05	data set 06	data set 07	data set 08	data set 09	data set 10	data set 11	data set 12
AG	4	*13.683*	*13.972*	*15.346*	*13.771*	*17.655*	*17.335*	*16.505*	*16.489*	*14.130*	*14.625*	*14.953*	*13.095*
	5	*13.687*	*13.981*	*15.358*	*13.767*	*17.664*	*17.342*	*16.508*	*16.489*	*14.152*	*14.641*	*14.975*	*13.115*
	6	*13.690*	*13.995*	*15.355*	*13.768*	*17.669*	*17.344*	*16.513*	*16.482*	*14.168*	*14.648*	*14.981*	*13.119*
	7	*13.695*	*13.994*	*15.354*	*13.767*	*17.664*	*17.338*	*16.514*	*16.484*	*14.173*	*14.650*	*14.987*	*13.120*
	8	*13.695*	*13.998*	*15.354*	*13.767*	*17.658*	*17.331*	*16.513*	*16.479*	*14.174*	*14.649*	*14.979*	*13.119*
ASD	4	*0.359*	*0.364*	*0.354*	*0.361*	*0.351*	*0.347*	*0.364*	*0.352*	*0.306*	*0.313*	*0.315*	*0.320*
	5	*0.359*	*0.364*	*0.354*	*0.361*	*0.351*	*0.347*	*0.364*	*0.352*	*0.306*	*0.314*	*0.315*	*0.321*
	6	*0.359*	*0.364*	*0.354*	*0.361*	*0.351*	*0.348*	*0.364*	*0.352*	*0.306*	*0.314*	*0.315*	*0.321*
	7	*0.359*	*0.364*	*0.354*	*0.361*	*0.351*	*0.347*	*0.364*	*0.352*	*0.307*	*0.314*	*0.315*	*0.321*
	8	*0.359*	*0.364*	*0.354*	*0.361*	*0.351*	*0.347*	*0.364*	*0.352*	*0.307*	*0.314*	*0.315*	*0.321*

to respective normal axial, normal coronal and Alzheimer's disease categories using scale 3, 4, and 5, respectively. Comparing Figs.2(d-1),(d-2),(d-3), which are the results using scale 4, to Figs. 2(c-1),(c-2),(c-3) and Figs. 2(e-1),(e-2),(e-3), which are the results using scales 5 and 3, respectively, we can find that the visibility of the anatomical structures in fused images in Figs. 2(d-x) is nearly as close to those in the MR as those using scale 5 and colors in Figs. 2(d-x) are also nearly as close to those in PET image as those using scale 3. Thus, we conclude that scale 4 is a good choice for achieving good result for both spatial and spectral fidelity.

Similarly, the selection of directional angle is also based on a trial result. In wavelet transform, using more directional angles in decomposition can extract high-frequency information from more directions, but the time complexity also increases. Thus, we conducted an experiment on the same 12 data sets of MR and PET brain images tested in the selection of decomposition scale using scale 4 with directional angle 4-8, respectively, and the same fusion rules for both high- and low-frequency subands. Note that we did not test cases with directional angle <4, as using too small directional angle (<4) cannot extract enough directional high-frequency information from the source image. Table I shows the spatial-quality performance of fusion results in terms of average gradient (AG) and average standard deviation (ASD), respectively, on these 12 data sets. As we can see in Table I, using directional angle 6 results in (2, 7) of (best, second best) AG out of these 12 datasets, and using directional angle 7

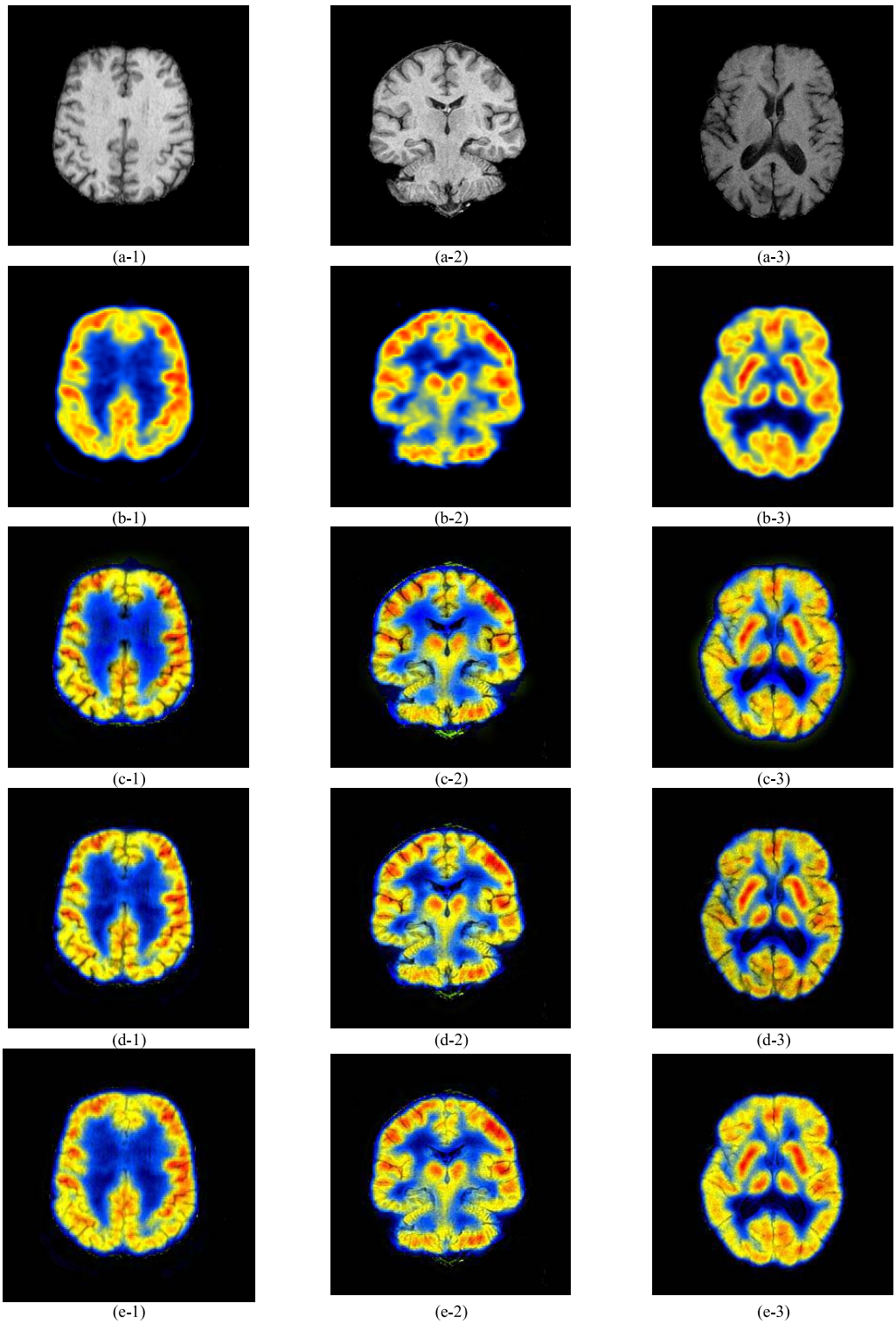

Fig. 2. Some examples of fusion results based on log-Gabor wavelet transform with different decomposition scales. (a-1)-(a-3) MR images. (b-1)-(b-3) PET images. (c-1)-(c-3) Fused results by using log-Gabor wavelet transform with decomposition scale 5. (d1)-(d3) Fused results by using log-Gabor wavelet transform with decomposition scale 4. (e1)-(e3) Fused results by using log-Gabor wavelet transform with decomposition scale 3.

results in (5, 3) of (best, second best) AG, although the value differences between the best and the second best are very small. In other words, using directional angles 6 and 7 results in approximately the same performance. As for measuring the fusion results in terms of ASD metric, the values are almost the same in using directional angles 4-8. Considering both spatial quality and time complexity, we conclude that directional angle 6 will be a good choice for our fusion scheme.Another important factor that affects the quality of fused images is the design of fusion rules for high- and low-frequency sub-bands of source images. The design of fusion rules is described in details in the following subsection.

2) The Design of Fusion Rules for High- and Low-Frequency Sub-Bands of Source Images: The fusion rules for high- and low-frequency sub-bands of source images play important role in the acquisition of high-quality resultant images. In the following sections, we describe the design of fusion rules for high- and low-frequency sub-bands of source images, respectively.

For high-frequency sub-bands, many wavelet-transform-based methods obtain new high-frequency sub-band coefficients of the fused image by directly preserving high-frequency sub-band coefficients from the high-spatial-resolution image, while discarding those from the low-spatial-resolution colorful image [21]. In our opinion, color changes are important visual information for the fusion of PET and MR brain images. To preserve anatomical structures while better keeping color changes in the fused image, high-frequency sub-bands from both the MR image and I-component of PET image should be considered. Therefore, in our fusion method, each high-frequency sub-band coefficient from the same location of MR image and I-component of PET image is selected by "Maximum Selection" (MS) rule based on the activity level of the considered coefficient. In [23], authors mentioned that "except for the LL band, which has all positive transform values, all the other bands contain transform values that are fluctuating around zero. The larger transform values in these bands correspond to sharper brightness changes and thus to the salient features in the image such as edges, lines, and region boundaries. Therefore, a good integration rule is the choose-max (CM) scheme, which means just picking the coefficient with the larger activity level and discarding the other." In fusion of PET and MR medical images, we hope to preserve sharper brightness (/color) changes from PET image and edges (/region boundaries) of anatomical structure from MR image. Therefore, using maximum selection rule (i.e. CM scheme as in [23]) is a good way to help us achieve this goal.

The activity level of the considered coefficient can be evaluated through a group of nearby coefficients or the considered coefficient itself. According to our observation, in high-frequency sub-bands, the response from the anatomical structures of MR image is sharper than that from the intensity changes of I component of PET image, so that high-frequency sub-band coefficients from the anatomical structures of MR image dominate the activity-level evaluation. Once nearby unrelated coefficients from the anatomical structures of MR image are taken into account, the activity-level estimation is no more accurate. In order to avoid incorrect activity-level estimation caused by nearby unrelated anatomical structures of MR image, the activity level of each coefficient is simply estimated by taking the absolute value of the considered coefficient itself in our strategy. Therefore, our fusion rule for high-frequency sub-bands is defined as follows:

$$W_F^h(x,y) = \begin{cases} W_P^h(x,y), & if\ |W_P^h(x,y)| \geq |W_M^h(x,y)| \\ W_M^h(x,y), & otherwise \end{cases} \quad (5)$$

where $W_F^h(x,y)$, $W_P^h(x,y)$ and $W_M^h(x,y)$ are the high-frequency sub-band coefficients at the location (x,y) of fused image, I-component of PET image, and MR image, respectively. We apply fusion rule in (5) to each coefficient of each high-frequency sub-band, and a new complete set of high-frequency sub-band coefficients for the fused image is then obtained.

For low-frequency sub-band fusion, we propose a new two-stage fusion rule to help our fused images appropriately preserve both color changes and anatomical structures. First, visibility measure of an image inspired from the human visual system (HSV) is utilized in our initial fusion process [29]. If the visibility of an image in a set of same-scene images is the maximum, then that image is less blurry among all. The visibility of an image L can be calculated as follows:

$$V(L) = \frac{1}{r \times c} \sum_{x=1}^{c} \sum_{y=1}^{r} \left(\frac{1}{\mu_L}\right)^{\alpha} \cdot \frac{|L(x,y) - \mu_L|}{\mu_L} \quad (6)$$

where r and c are the numbers of rows and columns in the image L, respectively. μ_L is the mean gray level of the image L andα is a visual constant ranging from 0.6 to 0.7. Further, the visibility of a low-frequency sub-band coefficient at location (x,y) of source image S can be evaluated as follows :

$$V_S^l(x,y) = V(W_S^l(N)) \quad (7)$$

where $S = P$ and M for the PET image and MR image, respectively. $W_S^l(N)$ is the set of low-frequency sub-band coefficients of source image S within window N of size $w \times w$ centering at location (x,y). To determine the low-frequency sub-band coefficient from which source image should be preserved, our initial fusion rule based on visibility measure is defined as follows:

$$W_V(x,y) = \begin{cases} W_P^l(x,y), & if\ V_P^l(x,y) \geq V_M^l(x,y) \\ W_M^l(x,y), & otherwise \end{cases} \quad (8)$$

where $W_P^l(x,y)$ and $W_M^l(x,y)$ are the low-frequency sub-band coefficients at the location (x,y) of I-component of PET image and MR image, respectively. Notice that the visibility of coefficients within anatomical structural regions is larger in MR image than in I-component of PET image. As a result, coefficients from I-component of PET image inside the anatomical structural regions can not be persevered, and subsequently color changes inside the anatomical structures regions will be missing when using fusion scheme only based on visibility measure. To overcome this color missing problem, the weighted-averaging strategy is introduced to improve fusion quality of our fusion method. Weighted-averaging fusion strategy is often used to combine low-frequency sub-band of source images and applying weighted-averaging fusion strategy to low-frequency sub-bands of MR image and I-component of PET image can be expressed as follows:

$$W_F^l(x,y) = w_p \times W_P^l(x,y) + (1 - w_p) \times W_M^l(x,y) \quad (9)$$

where W_F^l, W_P^l and W_M^l are the low-frequency sub-bands of the fused image, the I-component of PET image, and MR image, respectively. In addition, w_p is the weight assigned to the low-frequency sub-band of PET image. By giving different weight to each source image, the composite image therefore

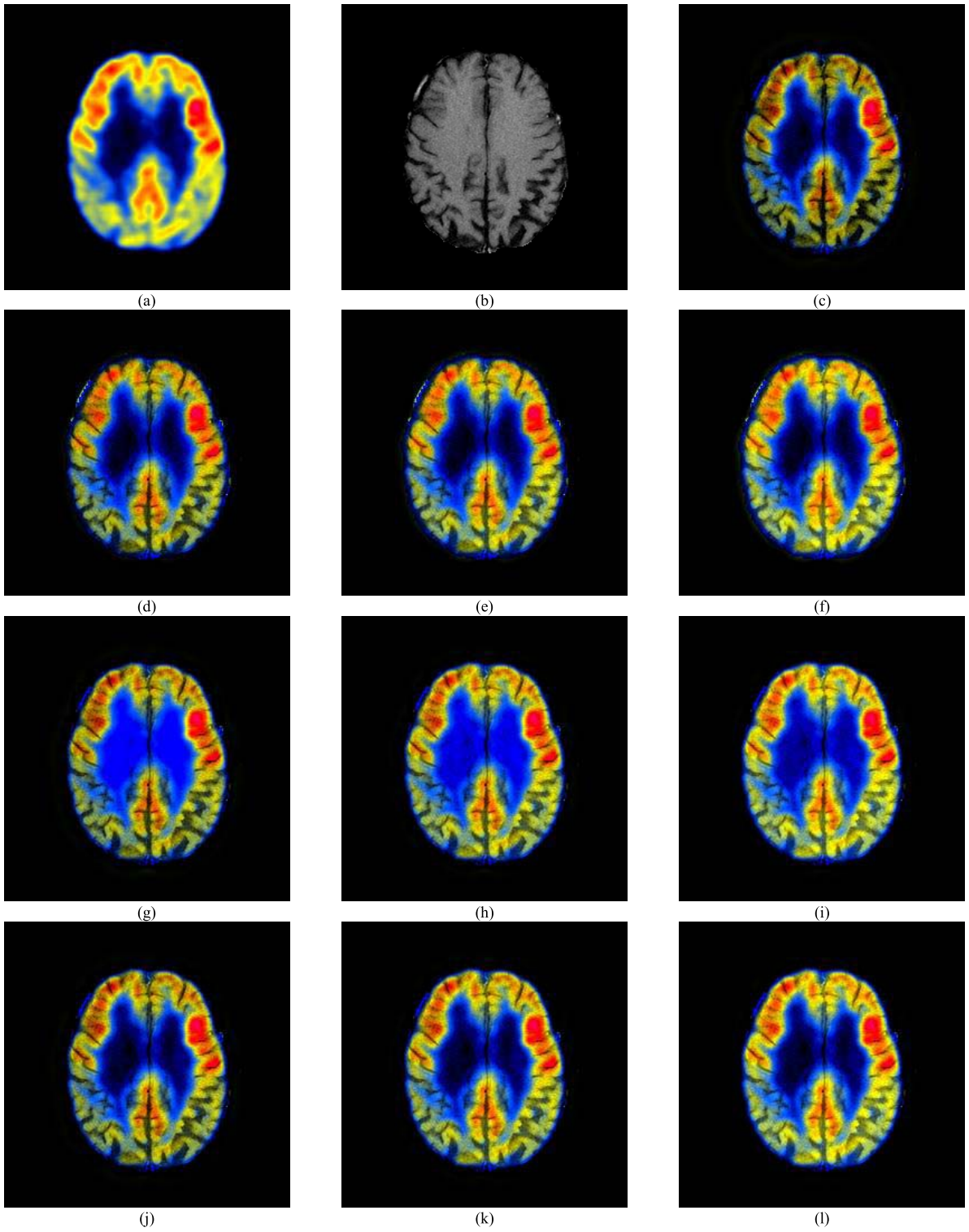

Fig. 3. Fusion results obtained by using different fusion rules. (a) PET image. (b) MR image. (c) Fusion result obtained by using maximum selection rule for high-frequency sub-bands fusion and only visibility measure for low-frequency sub-bands fusion. (d)-(f) Fusion results obtained by using high-frequency sub-bands from only MR and low-frequency sub-band from our two-stage fusion rule with $w_p = 0.3$, 0.5 and 0.7, respectively. (g)-(i) Fusion results obtained by using maximum selection rule for high-frequency sub-bands fusion and only weighted-averaging strategy for low-frequency sub-band fusion with $w_p = 0.3$, 0.5 and 0.7, respectively. (j)-(l) Fusion results obtained by using maximum selection rule for high-frequency sub-bands fusion and our two-stage fusion rule for low-frequency sub-band fusion with $w_p = 0.3$, 0.5 and 0.7, respectively.

preserve different amount of information from each source image. In general, giving more weight to the low-frequency sub-band of I-component of PET image makes fused images keep color changes better, but the visibility of anatomical structures in fused images is unsatisfactory. On the contrary, giving more weight to the low-frequency sub-band of MR

image improves preservation of anatomical structures, but colors in fused images are quite degraded. Nevertheless, colors may also be distorted even little weight is assigned to the low-frequency sub-band of MR image, if the gray-level distribution of MR image is rather different from that of I-component of PET image.

Fig. 3 demonstrates fusion results of applying different fusion rules. Fig. 3(c) is fusion result obtained by using maximum selection rule for high-frequency sub-bands fusion and only visibility measure for low-frequency sub-bands fusion. As we can see in Fig. 3 (c), anatomical structures are totally rendered and color changes outside those anatomical structures are moderately preserved. However, colors within those anatomical structures are covered up and missing, especially in the cerebrospinal fluid. Fig. 3(d)-(f) are fusion results obtained by using high-frequency sub-bands from only MR and low-frequency sub-band from our two-stage fusion rule with $w_p = 0.3$, 0.5 and 0.7, respectively. As we can see in (d)-(f), the red color is different from that of PET image no matter how much the weight w_p is assigned. The color difference between fusion result and PET image is due to the lack of high-frequency information from PET image in this fusion rule. Fig. 3(g)-(i) show fusion results obtained by using maximum selection rule for high-frequency sub-bands fusion and only weighted-averaging strategy for low-frequency sub-band fusion with $w_p = 0.3$, 0.5 and 0.7, respectively. As we can see in (g)-(i), the color is distorted, especially in the blue color in the center of the brain, no matter how much the weight w_p is assigned.

To take advantages of visibility measure and weighted-averaging strategy and avoid their drawbacks, we devise a new fusion rule for low-frequency sub-band as follows:

$$W_F^l(x,y) = w_p \times W_P^l(x,y) + (1 - w_p) \times W_V(x,y) \quad (10)$$

where W_F^l and W_P^l are the low-frequency sub-bands of the fused image and the I-component of PET image, respectively. W_V is the composite low-frequency sub-band obtained by fusion rule (8). The weighted-averaging strategy, as defined in equation (10), uses weight w_p to inject information of PET image so that color changes within anatomical structures can be appropriately rendered. Fig. 3 (j)-(l) show fusion results obtained by using maximum selection rule for high-frequency sub-bands fusion and our two-stage fusion rule for low-frequency sub-band fusion with $w_p = 0.3$, 0.5 and 0.7, respectively. As we can see in (j)-(l), the anatomical structures and color changes are rendered appropriately. Note that, comparing to the fusion results in (d) and (g), the anatomical structures are clear and the color changes are not distorted in our fusion result (j). In addition, the more the w_p is, the more the color changes are injected into anatomical structures, especially in the cerebrospinal fluid.

3) Our IHS+LG Fusion Method: Fig. 4 is the flow chart of our fusion method. At first, the PET image P is transformed to intensity (I_P), hue (H_P), and saturation (S_P) components by IHS model. The I-component of PET image, denoted IP, is decomposed by log-Gabor wavelet transform with 4 decomposition scales and 6 directional angles into

Algorithm 1: IHS+LG Fusion Method for the Fusion of PET and MR Brain Medical Images

Input: P- PET image
M- MR image
Output: F- a fused image

1. Transform PET image P from Red (R), Green (G), and Blue (B) channels to intensity (I_P), hue (H_P), and saturation (S_P) components by using IHS model.
2. Decompose MR image M and I-component I_P of PET image by using log-Gabor wavelet transform with 4 decomposition scales and 6 directional angles into high- and low-frequency sub-bands.
3. For each high-frequency sub-band, "Maximum Selection" (MS) rule based on the activity level of the considered coefficient is utilized as our fusion rule. Suppose $W_M^h(x,y)$ and $W_P^h(x,y)$ are the considered high-frequency coefficients of MR image M and I-component I_P of PET image P, respectively. Then, the activity level of the considered coefficient is simply evaluated by taking the absolute value of the considered coefficient itself. We preserve the coefficient with larger activity level as the coefficient of the fused image by using following fusion rule:
$$W_F^h(x,y) = \begin{cases} W_P^h(x,y), & if \ \left|W_P^h(x,y)\right| \geq \left|W_M^h(x,y)\right| \\ W_M^h(x,y), & otherwise \end{cases}$$
For the low-frequency sub-band, two-stage fusion rule is utilized. Suppose $W_F^l(x,y)$, $W_P^l(x,y)$ and $W_M^l(x,y)$ are the low-frequency sub-band coefficients at the location (x,y) of fused image F, I-component I_P of PET image, and MR image, respectively, then we initially combine coefficients based on visibility measure as follows:
$$W_V(x,y) = \begin{cases} W_P^l(x,y), & if \ V_P^l(x,y) \geq V_M^l(x,y) \\ W_M^l(x,y), & otherwise \end{cases}$$
where $V_P^l(x,y)$ and $V_M^l(x,y)$ are the visibility of the coefficient at location (x,y) of the low-frequency sub-band of MR image and I-component of PET image, respectively. After initial fusion, the advanced fusion based on weighted-averaging strategy is performed as follows:
$$W_F^l(x,y) = w_p \times W_P^l(x,y) + (1 - w_p) \times W_V(x,y)$$
where w_p is the weight assigned to the low-frequency sub-band of I-component of PET image.
4. Once the new complete set of high- and low-frequency sub-bands for the fused image is obtained, the new complete set $W_F = \{W_F^h, W_F^l\}$ is then reversely log-Gabor wavelet transformed to a new I-component I_F.
5. The fused I-component IF, along with unchanged HP and SP components of PET image, is transformed back to R, G, and B color channels to obtain the fused image F.
6. Return image F as result.

TABLE II
PERFORMANCE COMPARISON OF OUR FUSED IMAGES WITH HIGH-FREQUENCY INFORMATION FROM DIFFERENT SOURCES IN TERMS OF SD, AG, ASD, AND $Q^{AB/F}$ METRICS

High freq. sources	Only MR image				PET and MR image			
Metric / Data set	SD	AG	ASD	$Q^{AB/F}$	SD	AG	ASD	$Q^{AB/F}$
Data set 01	*6.6816*	*13.4688*	*0.3583*	*0.3812*	*5.3907*	*13.6726*	*0.3597*	*0.4201*
Data set 02	*5.8291*	*13.6451*	*0.3641*	*0.3854*	*4.6117*	*13.9487*	*0.3649*	*0.4279*
Data set 03	*7.2265*	*14.9193*	*0.3537*	*0.3795*	*5.9431*	*15.2425*	*0.3555*	*0.4185*
Data set 04	*7.2908*	*13.7502*	*0.3591*	*0.4010*	*6.1197*	*14.0044*	*0.3602*	*0.4273*
Data set 05	*7.5963*	*17.2522*	*0.3493*	*0.3723*	*6.4868*	*17.6442*	*0.3504*	*0.3976*
Data set 06	*7.8120*	*16.9742*	*0.3459*	*0.3675*	*6.6575*	*17.2672*	*0.3473*	*0.3968*
Data set 07	*7.4883*	*16.2540*	*0.3614*	*0.3642*	*6.3561*	*16.5485*	*0.3620*	*0.3918*
Data set 08	*7.7460*	*16.3361*	*0.3499*	*0.3982*	*6.6860*	*16.5921*	*0.3507*	*0.4188*
Data set 09	*6.4824*	*13.8311*	*0.3461*	*0.3967*	*4.6506*	*14.5109*	*0.3492*	*0.4550*
Data set 10	*5.9262*	*14.3348*	*0.3422*	*0.4149*	*4.3869*	*14.8962*	*0.3452*	*0.4588*
Data set 11	*5.9610*	*14.4444*	*0.3462*	*0.4228*	*4.4740*	*15.1115*	*0.3484*	*0.4640*
Data set 12	*5.7288*	*13.0035*	*0.3512*	*0.4274*	*3.8727*	*13.7608*	*0.3561*	*0.4896*

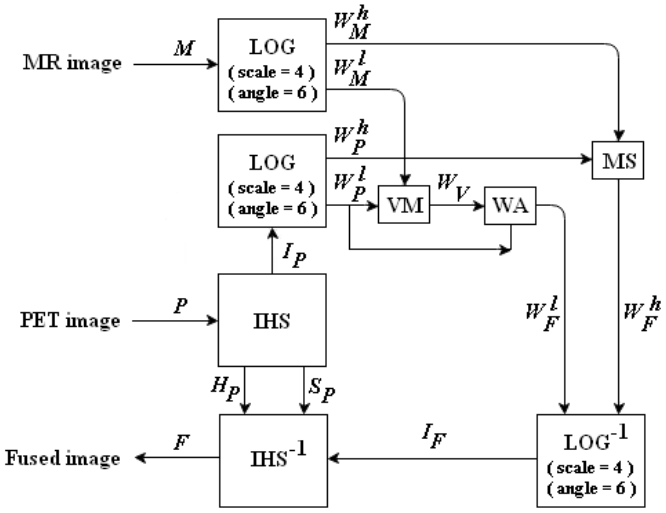

Fig. 4. The flow chart of our IHS+LG fusion method.

high- and low-frequency sub-bands, denoted W_P^h and W_P^l, respectively. Meanwhile, the MR image M is also decomposed by log-Gabor wavelet transform with 4 decomposition scales and 6 directional angles into high- and low-frequency sub-bands, denoted W_M^h and W_M^l, respectively. Each corresponding coefficient in the high-frequency sub-band of MR image (i.e. W_M^h) and I-component of PET image (i.e. W_P^h) is fused by "Maximum Selection" (MS) rule based on the activity level of the considered coefficient. Once all coefficients in all high-frequency sub-bands are processed, a new set of high-frequency sub-band coefficients for the fused image is then obtained, denoted W_F^h. For low-frequency sub-band, each corresponding coefficient in the low-frequency sub-band of MR image (i.e. W_M^l) and I-component of PET image (i.e. W_P^l) is initially integrated by fusion rule based on visibility measure, denoted "VM" for short. After initial combination, we can obtain a composite low-frequency sub-band W_V. Further, weighted-averaging fusion rule, denoted "WA" for short, is applied to the low-frequency sub-band of I-component of PET image (i.e. W_P^l) and the composite W_V. Once all coefficients in the low-frequency sub-band are processed after above two-stage fusion rules, we can obtain a new set of low-frequency sub-band coefficients for the fused image, denoted W_F^l. The new complete set of high- and low-frequency sub-bands coefficients for the fused image is then inversely log-Gabor wavelet transformed to obtain a fused I-component, denoted I_F. Finally, the fused I-component I_F, along with unchanged hue (H_P) and saturation (S_P) components of PET image, is inversely IHS transformed to obtain the fused image F. To clarify our fusion steps, the algorithm of our fusion method is proposed in Algorithm 1.

III. EXPERIMENTAL RESULTS AND ANALYSIS

In this paper, twelve data sets of PET and MR brain medical images downloaded from the web site (http://www.med.harvard.edu/aanlib/home.html) are used in our experiments. These twelve data sets consist of three types of brain images including normal axial, normal coronal and Alzheimer's disease brain images, and each type contains four pairs of PET and MR images of size 256 by 256 pixels with different content.

Note that, many registration methods have been proposed in literatures. Therefore, our study in this paper just focuses on the image fusion itself. In addition, the image sets from the web site of Harvard are well-registered so that we do not have to do registration before fusion task.

The assessment of fused image quality can either be subjective or objective. A subjective assessment is best performed by brain doctors to check if all valuable information is contained in the fused image visually. On the other hand, an objective assessment is based on various statistics of the fused image. In our study, four metrics are utilized for objective assessment including Spectral Discrepancy (SD) [22], Average Gradient (AG), Average Standard Deviation (ASD), and $Q_{AB/F}$ metric [34]. SD measures the spectral quality of a fused image by evaluating difference between the fused image and the PET image. The smaller the SD is, the closer the color of the fused image is to that of the PET image. AG measures spatial quality by evaluating the average of gradient in each R, G, and B channel of fused image within skull region (i.e. black pixels in the background are not considered). The larger the AG is,

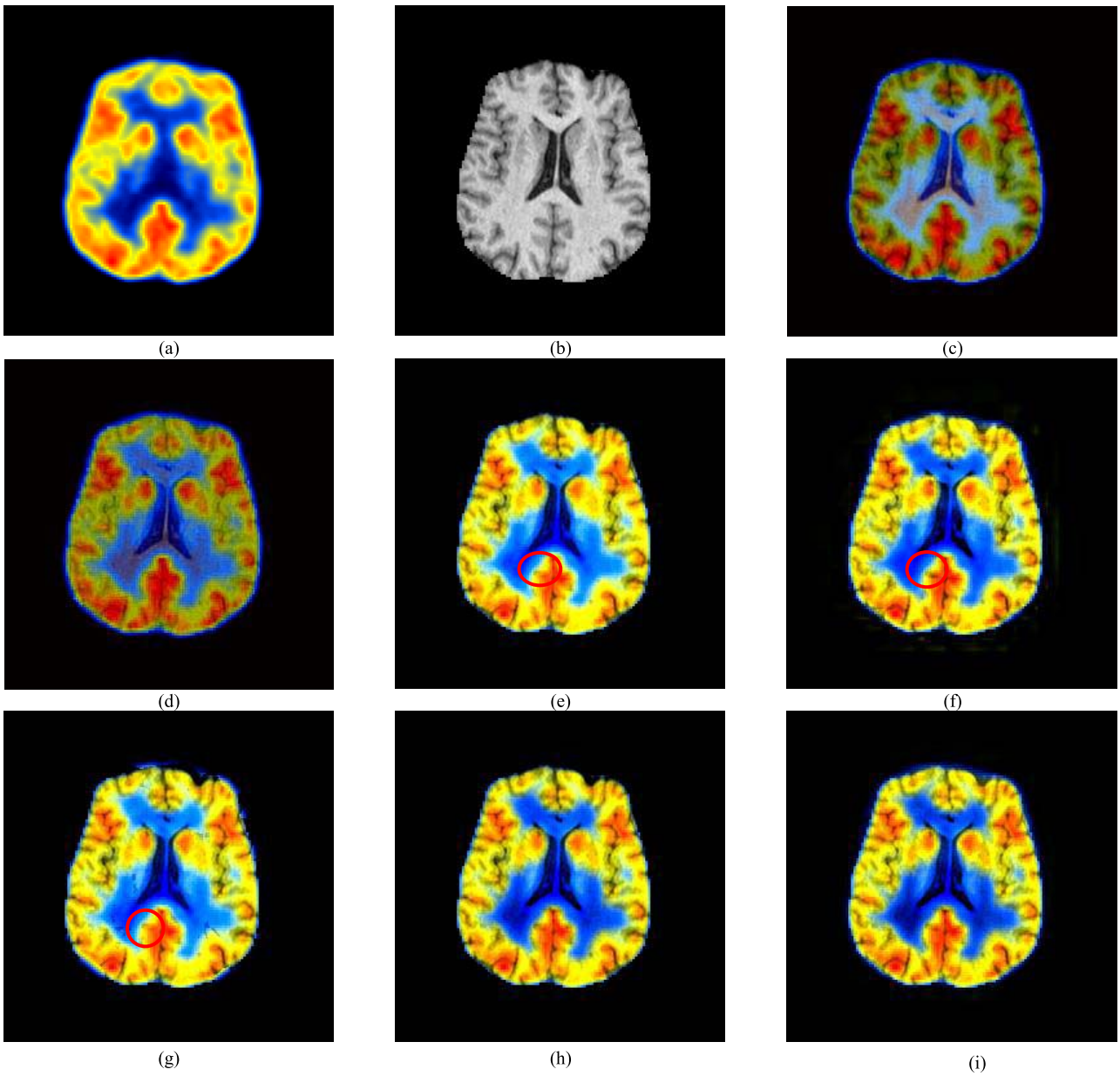

Fig. 5. Visual comparison for fusion results of normal axial brain images. (a) PET image. (b) MR image. (c) Result of PCA method. (d) Result of PCA+DWT method. (e) Result of IHS-substitution method. (f) Result of IHS+DWT method. (g) Result of our IHS+GF method. (h) Result of IHS+FT method. (i) Result of our IHS+LG method.

the better the spatial quality of the fused image within skull region is. ASD measures spatial quality by taking the average of standard deviation in each R, G, and B channel of the fused image within skull region. The larger the ASD is, the better the spatial quality of the fused image within skull region is. $Q^{AB/F}$ metric utilizes edge information, which is important visual information, to measure the similarity between the fused image and the input source images pixel by pixel. Larger value of $Q^{AB/F}$ indicates that the fused image and input source images are more similar.

A. Fusion Effect From Considering High-Frequency Information of PET Image

As we mentioned in Section 3, many traditional wavelet-transform-based fusion methods discard high-frequency information of low-spatial-resolution images in their fusion process. In our opinion, the color changes of PET image are important visual information for the fusion of PET and MR brain medical images. Therefore, to construct high-quality resultant images with better preservation of color changes of PET image, the intensity changes of I component of PET image respond in the high-frequency sub-bands should be also considered in fusion process.

To demonstrate the fusion effect from considering high-frequency information of PET image, we conduct our fusion method based on two different fusion rules for high-frequency sub-bands. One is the fusion rule that preserves high-frequency sub-bands coefficients from only the MR image, the other is the fusion rule defined in (5) that preserves high-frequency sub-bands coefficients from both the MR and PET images. Besides, we fix our weight $w_p = 1.0$ for the low-frequency sub-band fusion. As we can see in equation (10), once we use

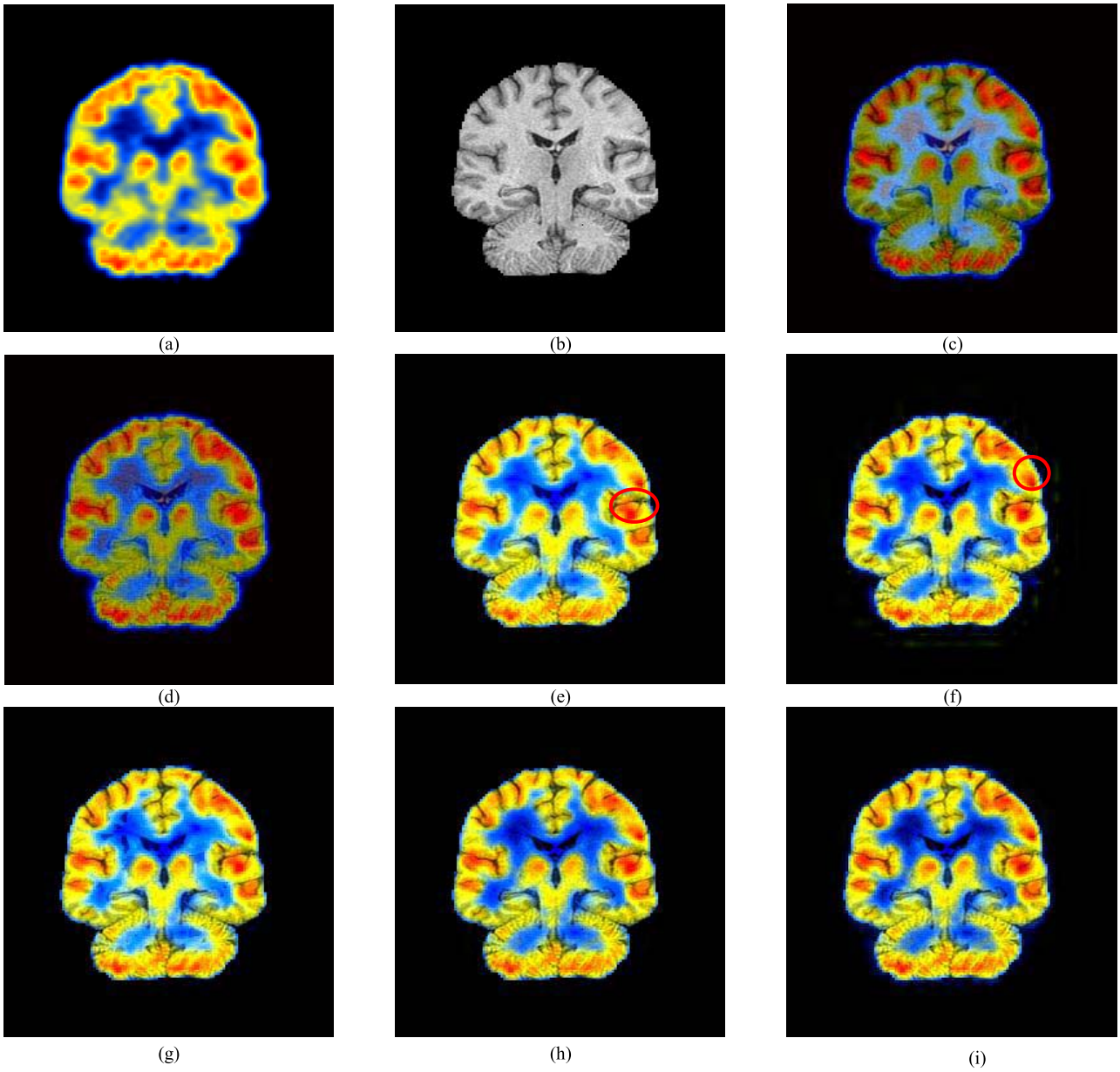

Fig. 6. Visual comparison for fusion results of normal coronal brain images. (a) PET image. (b) MR image. (c) Result of PCA method. (d) Result of PCA+DWT method. (e) Result of IHS-substitution method. (f) Result of IHS+DWT method. (g) Result of our IHS+GF method. (h) Result of IHS+FT method. (i) Result of our IHS+LG method.

$w_p = 1.0$ for low-frequency sub-band fusion, the $W_F^l(x, y)$ will be the $W_P^l(x, y)$ itself, which is the low-frequency sub-band of I-component of PET image, so that the low-frequency and high-frequency coefficients from I-component of PET image can be completely combined and color changes of PET image are preserved and really evaluated by quantitative measures in fusion results.

In this experiment, twelve pairs of PET and MR brain images are used as testing data sets. These twelve data sets consisting of three types of brain images with different content are labeled as data set 01-04 for normal axial brain images, data set 05-08 for normal coronal brain images, and data set 09-12 for Alzheimer's disease brain images. Table II shows the performance comparison of our fused images with high-frequency information from different sources in terms of SD, AG, ASD, and $Q^{AB/F}$ metrics. As we can see in Table II, it is obvious that SD values of fused images with high-frequency information from both the MR and PET images are much smaller than those from only the MR image. This indicates that the introduction of high-frequency information from the PET image indeed help our fusion method keep color changes better. In terms of AG and ASD, the AG and ASD values of fused images with high-frequency information from both the MR and PET images are a little larger than those from only the MR image. This indicates that preserving high-frequency information from the PET image into the fused image increases the gray-level changes in each individual R, G, and B channel. Moreover, in terms of $Q^{AB/F}$ metrics, the $Q^{AB/F}$ values of fused images with high-frequency information from both the MR and PET images are quite larger

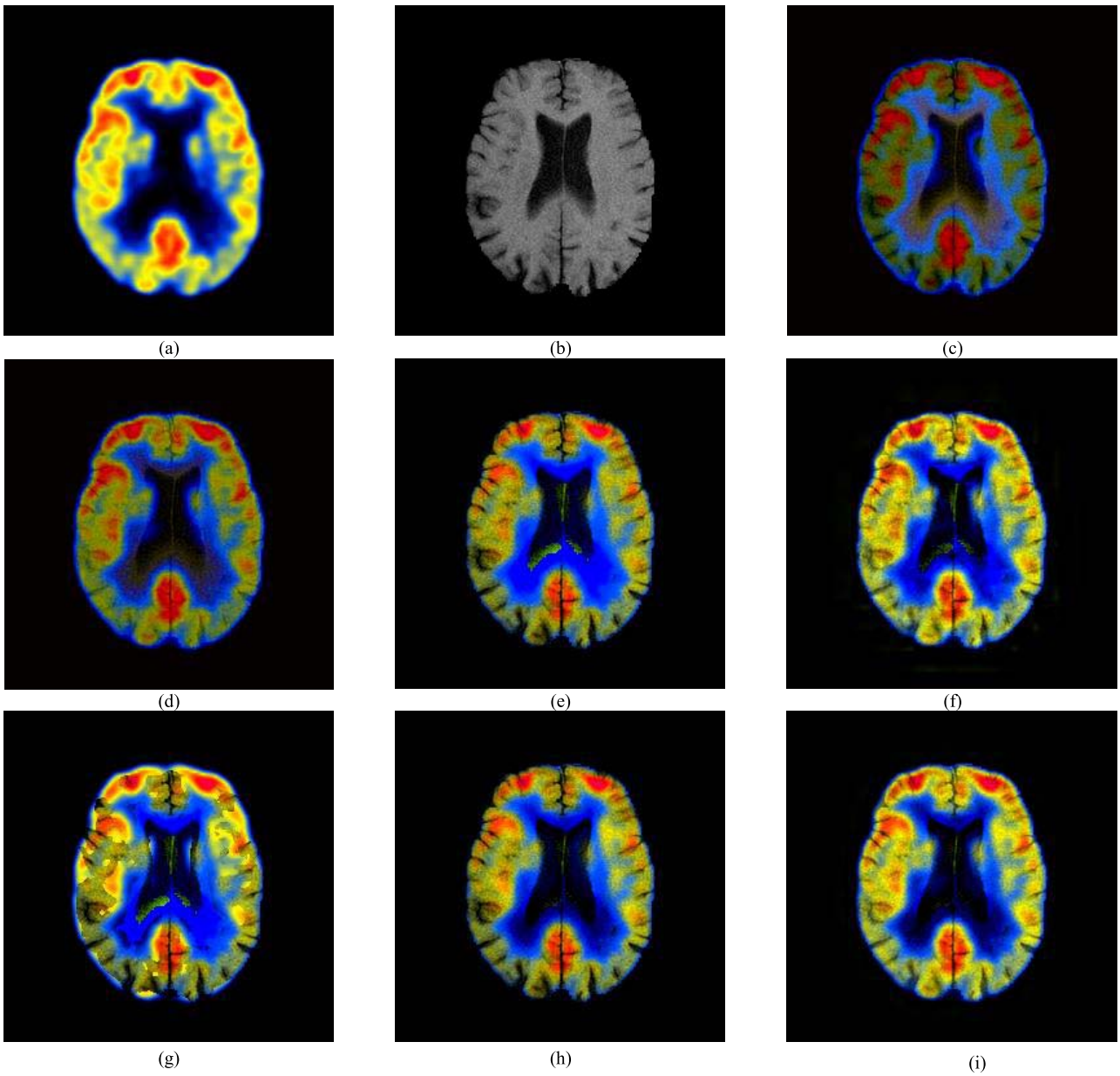

Fig. 7. Visual comparison for fusion results of Alzheimer's disease brain images. (a) PET image. (b) MR image. (c) Result of PCA method. (d) Result of PCA+DWT method. (e) Result of IHS-substitution method. (f) Result of IHS+DWT method. (g) Result of our IHS+GF method. (h) Result of IHS+FT method. (i) Result of our IHS+LG method.

than those from only the MR image. Therefore, preserving high-frequency information from the PET image into the fused image obviously improves the similarity between our fused image and input source images.

B. Visual Comparison of Fusion Results

In this experiment, PET and MR brain medical images, including normal axial, normal coronal, and Alzheimer's disease brain images, shown in Fig. 5-7 (a) and (b) are used for the visual comparison. Fusion results obtained by using different methods, including (c) PCA method, (d) PCA+DWT based on PCA and simple wavelet transform (Daubechies 2 wavelet transform), (e)-IHS-substitution method, (f)-IHS+DWT method based on IHS model and simple wavelet transform (Daubechies 2 wavelet transform), (g)-IHS+GF method based on IHS model and Gabor filters (8 directional angles), (h)-IHS+FT method based on IHS model and framelet transform [29], and (i)-our IHS+LG method, are shown in Fig. 5-7 (c)-(i). As we can see in Fig. 5, compare with source images in Fig. 5 (a) and (b), blue color shade in Fig. 5 (c)-PCA method is distorted seriously, and it is improved a little bit but still distorted in Fig. 5 (d)- PCA+DWT method. In addition, blue color shade in Fig. 5 (e)-IHS-substitution method is lighter and some anatomical structures are missing within the red-circle areas. Similarly, blue color shade in Fig. 5 (f)-IHS+DWT method is still lighter than that in Fig. 5 (a) and the visibility

TABLE III
PERFORMANCE COMPARISON OF FUSED IMAGES OBTAINED BY PCA, PCA+DWT, IHS+FT METHODS AND OUR IHS+LG METHOD IN TERMS OF SD, AG, ASD, AND $Q^{AB/F}$ METRICS

Methods	PCA				PCA+DWT				IHS+FT				Our IHS+LG			
Metric / Data set	SD	AG	ASD	$Q^{AB/F}$	SD	AG	ASD	$Q^{AB/F}$	SD	AG	ASD	$Q^{AB/F}$	SD	AG	ASD	$Q^{AB/F}$
Data set 01	*21.8949*	*9.4621*	*0.2254*	*0.3855*	*15.0223*	*9.8571*	*0.2471*	*0.3970*	*8.5913*	*13.3743*	*0.3306*	*0.3748*	*6.1858*	*13.6901*	*0.3594*	*0.4186*
Data set 02	*22.4176*	*9.6253*	*0.2233*	*0.3775*	*15.0464*	*10.1338*	*0.2452*	*0.4024*	*7.1517*	*13.7013*	*0.3413*	*0.3828*	*5.1094*	*13.9945*	*0.3640*	*0.4284*
Data set 03	*22.0360*	*10.7047*	*0.2401*	*0.4010*	*16.0650*	*11.1281*	*0.2537*	*0.4013*	*9.1639*	*15.1116*	*0.3294*	*0.3809*	*6.7158*	*15.3552*	*0.3542*	*0.4184*
Data set 04	*21.9488*	*9.9271*	*0.2459*	*0.4070*	*16.0306*	*10.2165*	*0.2576*	*0.4105*	*8.9201*	*13.0934*	*0.3525*	*0.3894*	*6.7821*	*13.7682*	*0.3613*	*0.4230*
Data set 05	*21.4217*	*12.0426*	*0.2271*	*0.3967*	*15.9430*	*12.6560*	*0.2481*	*0.3940*	*8.4966*	*17.2853*	*0.3230*	*0.3751*	*6.8071*	*17.6686*	*0.3513*	*0.3987*
Data set 06	*20.5497*	*11.8181*	*0.2297*	*0.3999*	*15.6020*	*12.2766*	*0.2506*	*0.3924*	*9.1473*	*17.0763*	*0.3195*	*0.3712*	*7.1219*	*17.3436*	*0.3475*	*0.3975*
Data set 07	*23.5013*	*11.4812*	*0.2130*	*0.4015*	*16.5952*	*11.9396*	*0.2384*	*0.3861*	*8.3880*	*16.1125*	*0.3369*	*0.3662*	*6.6611*	*16.5128*	*0.3643*	*0.3924*
Data set 08	*20.3564*	*11.5016*	*0.2469*	*0.4029*	*15.5300*	*12.0523*	*0.2592*	*0.4110*	*8.9887*	*15.9189*	*0.3379*	*0.3977*	*7.0793*	*16.4816*	*0.3521*	*0.4188*
Data set 09	*24.3748*	*8.9802*	*0.1933*	*0.3681*	*17.0107*	*9.9476*	*0.2288*	*0.4278*	*15.7603*	*12.7093*	*0.2454*	*0.3490*	*8.1228*	*14.1684*	*0.3064*	*0.4370*
Data set 10	*24.6783*	*9.3718*	*0.1985*	*0.3704*	*18.6110*	*10.3294*	*0.2382*	*0.4266*	*13.9061*	*13.4788*	*0.2591*	*0.3685*	*7.4971*	*14.6476*	*0.3137*	*0.4441*
Data set 11	*26.5500*	*9.7253*	*0.1939*	*0.3698*	*19.5805*	*10.7309*	*0.2312*	*0.4305*	*14.8607*	*13.6554*	*0.2612*	*0.3802*	*7.9671*	*14.9807*	*0.3152*	*0.4525*
Data set 12	*23.3011*	*8.7820*	*0.1976*	*0.3708*	*16.6259*	*9.7369*	*0.2384*	*0.4423*	*13.1057*	*11.3935*	*0.2724*	*0.3666*	*6.8670*	*13.1189*	*0.3206*	*0.4660*

of some anatomical structures is low within the red-circle areas. Fig. 5 (g)-IHS+GF method has poor structural visibility in some areas, and blue color shade is obviously lighter than original PET image in Fig. 5 (a). Fig. 5 (h)-IHS+FT method has better structural visibility in some areas than Fig. 5 (c)-(f), however, blue color shade is still a little bit lighter than original PET image in Fig. 5 (a). It is obvious that Fig. 5 (i)-our IHS+LG method preserves appropriately both anatomical structures and color changes, and therefore has better visual effect than other methods. Fusion results shown in Fig. 6 also demonstrate that fused image obtained by our method is better than those obtained by other methods in visual perception. From Fig. 7, it is obvious that (c)-PCA method, (d)-PCA+DWT method, (e)-IHS-substitution method, (f)-IHS+DWT method and (g)-IHS+GF method exhibit serious color distortion, especially in blue color shade. Such color distortion would mislead doctors in diagnosis and treat them as disorders. Fig. 7 (h)-IHS+FT method has good visibility of anatomical structures in some areas, but color of PET image is not preserved well within those anatomical structures, and distortion in blue color shade still can be spotted. Again, our fused image shown in Fig. 7 (i) appropriately presents the anatomical structures of MR image and the color changes of PET image, and therefore has better visual effect than fused images obtained by other methods. The main reasons leading to the better visual effect in our fusion method is the usage of log-Gabor wavelet transform with suitable decomposition scales and our fusion rules for high- and low-frequency sub-bands. Because we utilize the log-Gabor wavelet transform with suitable decomposition scales to decompose source images, the high-frequency information of source images is more separated from the low-frequency information, and our fusion rules sophisticatedly treat those high- and low-frequency information and better preserve them into fused images.

C. Performance Comparison via Quantitative Measurements

Besides visual comparison, we also compare the fusion performance of our IHS+LG method with the state-of-the-art IHS+FT method [29] as well as PCA method and PCA+DWT method [17], [19], based on twelve data sets in terms of four quantitative measurements. To fairly judge these fusion methods, the visual constant $\alpha = 0.65$ and the window N of size 3 by 3 for the visibility evaluation are adopted in both the IHS+FT method and IHS+LG method. Moreover, in PCA+DWT method, daubechies 2 wavelet with decomposition scale 3 is used. In addition, decomposition scale 3 for the framelet transform that helps IHS+FT method obtain high-quality fused images, and weight $w_p = 0.5$ that helps our IHS+LG method obtain fused images with appropriate color changes and anatomical structures, are used in this experiment. The quantitative performance of twelve fused images obtained by PCA, PCA+DWT, IHS+FT method and our IHS+LG method in terms of SD, AG, ASD, and $Q^{AB/F}$ metrics is shown in Table III, where data sets 01-04 are normal axial brain images, data sets 05-08 are normal coronal brain images, and data sets 09-12 are Alzheimer's disease brain images. From Table III, we can see that SD values of fused images obtained by our IHS+LG method are much smaller than those obtained by PCA, PCA+DWT and IHS+FT methods. As we mentioned above, SD measures the color difference between the fused image and the input PET image. Therefore, we can conclude that our fused images are closer to the input PET images and better preserve color changes of PET image with less color distortion. In terms of AG and ASD, fused images of our IHS+LG method have larger AG and ASD values than those of compared methods because fused images of our method better preserve anatomical structures of MR images and color changes of PET. Moreover, in terms of $Q^{AB/F}$ metrics, the performance of fused images achieved by our method is better than that of compared methods. This indicates that fused images obtained by our method are more similar to both the input images than those obtained by IHS+FT method.

D. Discussion

In clinical examination, doctors often have to examine PET and MR image in different weight according to their need. From above experimental results, we know that each fusion method we compared offers no flexibility for doctors to adjust

fusion result to meet their preference. Each fusion method can only generate one fusion result from each pair of source images such that doctors can not examine the fused image in arbitrary weight between PET and MR images. On the contrary, in our new fusion method, our two-stage fusion rule for the low-frequency sub-bands provides us an easy way to adjust the amount of PET color changes (MR anatomical structures) rendering in the fusion results. If doctors want to examine the fused image with more clear PET color changes, they can set larger weight w_p for the fusion of low-frequency sub-band. Therefore, our fusion method is more suitable for doctors in clinical practice.

The limitation of our method is that we assume source images are well-registered and we do not have any special preprocessing scheme to deal with unregistered source images. Once the source images are not registered well, our fusion scheme may generate artifacts in fusion results as other previously-proposed methods in literatures.

For the future recommendations, we know that our fusion scheme is a little bit time-consuming because the coefficients from both MR image and I-component of PET image are considered for high-frequency sub-bands fusion, and two-stage fusion rules based on visibility measure and weighted-averaging strategy is used for low-frequency sub-bands fusion. Therefore, how to seed up our fusion scheme is a challenging issue for our future research.

IV. Conclusions

In this paper, we propose a new fusion method for the fusion of PET and MR brain images, denoted IHS+LG, based on IHS model and log-Gabor wavelet transform with suitable decomposition scales and fusion rules. In our method, MR image and I-component of PET image, which is obtained from transforming PET image by IHS model, are decomposed into high- and low-frequency sub-bands by log-Gabor wavelet transform with four decomposition scales and six directional angles. Both the high-frequency sub-bands of MR image and I-component of PET image are considered and then fused by "Maximum Selection" (MS) fusion rule based on the simple absolute value of the considered coefficient. By considering the high-frequency sub-bands of I-component of PET image, color changes are better preserved in the fused image. Meanwhile, the low-frequency sub-bands of MR image and I-component of PET image are integrated by our two-stage fusion rules based on the visibility measure and weighted-averaging fusion strategy. With our two-stage fusion rule, both anatomical structures and color changes are appropriately preserved in the fused image while color distortion is effectively reduced. Experimental results on twelve data sets, including normal axial, normal coronal, and Alzheimer's disease brain images, demonstrate that our IHS+LG method is better than state-of-the-art IHS+FT method not only in visual perception but also in terms of SD, AG, ASD, and $Q^{AB/F}$ metrics.

References

[1] D. Acharjya and A. Anitha, "A comparative study of statistical and rough computing models in predictive data analysis," *Int. J. Ambient Comput. Intell.*, vol. 8, no. 2, pp. 32–51, 2017.

[2] D. R. Kishor and N. B. Venkateswarlu, "Hybridization of expectation-maximization and K-means algorithms for better clustering performance," *Cybern. Inf. Technol.*, vol. 16, no. 2, pp. 16–34, Jun. 2016. [Online]. Available: http://dl.acm.org/citation.cfm?id=3060245

[3] S. Hemalatha and S. M. Anouncia, "A computational model for texture analysis in images with fractional differential filter for texture detection," *Int. J. Ambient Comput. Intell.*, vol. 7, no. 2, pp. 93–113, 2016. [Online]. Available: https://www.igi-global.com/book/biometrics-concepts-methodologies-tools-applications/154882

[4] S. Li, X. Kang, L. Fang, J. Hu, and H. Yin, "Pixel-level image fusion: A survey of the state of the art," *Inf. Fusion*, vol. 33, pp. 100–112, Jan. 2017.

[5] A. Toet, L. J. Van Ruyven, and J. M. Valeton, "Merging thermal and visual images by a contrast pyramid," *Opt. Eng.*, vol. 28, no. 7, pp. 789–792, 1989.

[6] M. I. Smith and J. P. Heather, "A review of image fusion technology in 2005," *Proc. SPIE*, vol. 5782, pp. 29–45, Mar. 2005. [Online]. Available: https://www.spiedigitallibrary.org/conference-proceedings-of-spie/5782/1/A-review-of-image-fusion-technology-in-2005/10.1117/12.597618.pdf?SSO=1

[7] V. Barra and J.-Y. Boire, "A general framework for the fusion of anatomical and functional medical images," *NeuroImage*, vol. 13, pp. 410–424, Mar. 2001.

[8] D. Wang *et al.*, "Image fusion incorporating parameter estimation optimized Gaussian mixture model and fuzzy weighted evaluation system: A case study in time-series plantar pressure data set," *IEEE Sensors J.*, vol. 17, no. 5, pp. 1407–1420, Mar. 2017.

[9] L. Moraru, S. Moldovanu, L. T. Dimitrievici, F. Shi, A. S. Ashour, and N. Dey, "Quantitative diffusion tensor magnetic resonance imaging signal characteristics in the human brain: A hemispheres analysis," *IEEE Sensors J.*, vol. 17, no. 15, pp. 4886–4893, Aug. 2017.

[10] A. Tharwat, T. Gaber, Y. M. Awad, N. Dey, and A. E. Hassanien, "Plants identification using feature fusion technique and bagging classifier," in *Proc. 1st Int. Conf. Adv. Intell. Syst. Informat. (AISI)*, Beni Suef, Egypt, Nov. 2015, pp. 461–471.

[11] S. Daneshvar and H. Ghassemian, "MRI and PET image fusion by combining IHS and retina-inspired models," *Inf. Fusion*, vol. 11, pp. 114–123, Apr. 2010.

[12] A. L. Grosu *et al.*, "Reirradiation of recurrent high-grade gliomas using amino acid PET (SPECT)/CT/MRI image fusion to determine gross tumor volume for stereotactic fractionated radiotherapy," *Int. J. Radiat. Oncol. Biol. Phys.*, vol. 63, no. 2, pp. 511–519, 2005.

[13] J. Suri *et al.*, "Real time four different image registration techniques in temporal intravascular ultrasound (IVUS) videos: Importance in cardiovascular interventional ultrasound procedures," *Ultrasound Med. Biol.*, vol. 41, no. 4, p. 1, 2015.

[14] S. Chakraborty, P. K. Patra, P. Maji, A. S. Ashour, and N. Dey, "Image registration techniques and frameworks: A review," in *Applied Video Processing in Surveillance and Monitoring Systems*. Hershey, PA, USA: IGI Publishing, 2017, ch. 5. [Online]. Available: http://dl.acm.org/citation.cfm?id=3122402

[15] B. Zitova and J. Flusser, "Image registration methods: A survey," *Image Vis. Comput.*, vol. 21, pp. 977–1000, Apr. 2003.

[16] H. Lee, J. Lee, N. Kim, I. K. Lyoo, and Y. G. Shin, "Robust and fastshell registration in PET and MR/CT brain images," *Comput. Biol. Med.*, vol. 39, pp. 961–977, Sep. 2009.

[17] M. G. Audicana, J. L. Saleta, R. G. Catalan, and R. Garcia, "Fusion of multispectral and panchromatic images using improved IHS and PCA mergers based on wavelet decomposition," *IEEE Trans. Geosci. Remote Sens.*, vol. 43, no. 9, pp. 1291–1299, Sep. 2004.

[18] P. S. J. Chavez and A. Y. Kwarteng, "Extracting spectral contrast in Landsat thematic mapper image data using selective principal component analysis," *Photogramm. Eng. Remote Sens.*, vol. 55, no. 3, pp. 339–348, 1989.

[19] T. Tu, S. Su, H. Shyu, and P. S. Huang, "A new look at IHS-like image fusion methods," *Inf. Fusion*, vol. 11, pp. 177–186, Jun. 2001.

[20] Y. Chibani and A. Houacine, "Redundant versus orthogonal wavelet decomposition for multisensor image fusion," *Pattern Recognit.*, vol. 36, pp. 879–887, Oct. 2003.

[21] J. Nunez, X. Otazu, O. Fors, A. Prades, V. Pala, and R. Arbiol, "Multiresolution-based image fusion with additive wavelet decomposition," *IEEE Trans. Geosci. Remote Sens.*, vol. 37, no. 3, pp. 1204–1211, May 1999.

[22] Z. Li, Z. Jing, X. Yang, and S. Sun, "Color transfer based remote sensing image fusion using non-separable wavelet frame transform," *Pattern Recognit. Lett.*, vol. 26, no. 13, pp. 2006–2014, 2005.

[23] G. Pajares and J. M. de la Cruz, "A wavelet-based image fusion tutorial," *Pattern Recognit.*, vol. 37, no. 9, pp. 1855–1872, 2004.
[24] M. N. Do and M. Vetterli, "The contourlet transform: An efficient directional multiresolution image representation," *IEEE Trans. Image Process.*, vol. 14, no. 12, pp. 2091–2106, Dec. 2005.
[25] A. L. da Cunha, J. Zhou, and M. N. Do, "The nonsubsampled contourlet transform: Theory, design, and applications," *IEEE Trans. Image Process.*, vol. 15, no. 10, pp. 3089–3101, Oct. 2006.
[26] T. Li and Y. Wang, "Biological image fusion using a NSCT based variable-weight method," *Inf. Fusion*, vol. 12, no. 2, pp. 85–92, 2011.
[27] C. K. Chui and W. He, "Compactly supported tight frames associated with refinable functions," *Appl. Comput. Harmon. Anal.*, vol. 8, no. 3, pp. 293–319, 2000.
[28] I. W. Selesnick and A. F. Abdelnour, "Symmetric wavelet tight frames with two generators," *Appl. Comput. Harmon. Anal.*, vol. 17, no. 2, pp. 211–225, 2004.
[29] G. Bhatnagar, Q. M. Wu, and L. Zheng, "Human visual system inspired multi-modal medical image fusion framework," *Expert Syst. Appl.*, vol. 40, no. 5, pp. 1708–1720, 2013.
[30] V. S. N. Prasad and J. Domke, "Gabor filter visualization," Tech. Rep., Univ. Maryland, College Park, MD, USA, 2005.
[31] S. Fischer, F. Šroubek, L. Perrinet, R. Redondo, and G. Cristóbal, "Self-invertible 2D log-Gabor wavelets," *Int. J. Comput. Vis.*, vol. 75, no. 2, pp. 231–246, Nov. 2007.
[32] S. Fischer, R. Redondo, and G. Cristóbal, "How to construct log-Gabor filters?" Inst. Optica, Madrid, Spain, Tech. Rep., Jul. 2009. [Online]. Available: http://www.academia.edu/1316161/How_to_construct_log-Gabor_Filters
[33] R. Redondo, F. Šroubek, S. Fischer, and G. Cristóbal, "Multifocus image fusion using the log-Gabor transform and a multisize windows technique," *Inf. Fusion*, vol. 10, no. 2, pp. 163–171, 2009.
[34] C. S. Xydeas and V. Petrović, "Objective image fusion performance measure," *Electron. Lett.*, vol. 36, no. 4, pp. 308–309, 2000.

Cheng-I Chen was born in Changhua County, Taiwan, in 1981. He received the B.S. degree in computer science from Tunghai University, Taichung, Taiwan, in 2004, and the M.S. degree in computer science and engineering from National Chung Hsing University, Taichung, Taiwan, in 2006, where he is currently pursuing the Ph.D. degree in computer science and engineering. His research interests including multi-focus image fusion and brain medical image fusion, and he had published research papers about image fusion in several conferences, including the IEEE International Symposium on Bioelectronics and Bioinformatics in 2014.

Mr. Chen received the Best Paper Award for the study of brain medical image fusion at the IADIS Multi Conference on Computer Science and Information Systems 2011CGVCVIP, Rome, Italy, 2011.